

OptiRoulette Optimizer: A New Stochastic Meta-Optimizer for up to 5.3x Faster Convergence

Stamatis Mastromichalakis
Independent Researcher, tmnetworks.gr
stamatis@tmnetwork.gr
 <https://orcid.org/0000-0003-1713-5078>

This paper presents OptiRoulette, a stochastic meta-optimizer that selects update rules during training instead of fixing a single optimizer. The method combines warmup optimizer locking, random sampling from an active optimizer pool, compatibility-aware learning-rate scaling during optimizer transitions, and failure-aware pool replacement. OptiRoulette is implemented as a drop-in, `torch.optim.Optimizer`-compatible component and packaged for pip installation. We report completed 10-seed results on five image-classification suites: CIFAR-100, CIFAR-100-C, SVHN, Tiny ImageNet, and Caltech-256. Against a single-optimizer AdamW baseline, OptiRoulette improves mean test accuracy from 0.6734 to 0.7656 on CIFAR-100 (+9.22 percentage points), 0.2904 to 0.3355 on CIFAR-100-C (+4.52), 0.9667 to 0.9756 on SVHN (+0.89), 0.5669 to 0.6642 on Tiny ImageNet (+9.73), and 0.5946 to 0.6920 on Caltech-256 (+9.74). Its main advantage is convergence reliability at higher targets: it reaches CIFAR-100/CIFAR-100-C 0.75, SVHN 0.96, Tiny ImageNet 0.65, and Caltech-256 0.62 validation accuracy in 10/10 runs, while the AdamW baseline reaches none of these targets within budget. On shared targets, OptiRoulette also reduces time-to-target (e.g., Caltech-256 at 0.59: 25.7 vs 77.0 epochs). Paired-seed deltas are positive on all datasets; CIFAR-100-C test ROC-AUC is the only metric not statistically significant in the current 10-seed study.

Key words: *stochastic optimizer selection, LR scaling, optimizer pool, dynamic optimizer switching, convergence acceleration, deep neural network optimization*

Disclaimer: The OptiRoulette name refers exclusively to a machine-learning optimizer and has no affiliation, sponsorship, or technical relation to roulette manufacturers, casinos, or any physical/software gambling products or services.

Author: Stamatis Mastromichalakis

Official Repository: [GitHub Repository](#)

1. Introduction

Optimizer choice remains a first-order determinant of deep-network training efficiency and final quality. In current practice, however, training typically relies on a single fixed optimizer (e.g., SGD-family or Adam-family) across all epochs, despite well-known stage-dependent behavior: adaptive methods often provide strong early progress, while non-adaptive methods may provide stronger late-stage generalization. This stage mismatch motivates optimizer policies that can evolve during training rather than remain static.

Prior work has explored several directions toward this goal. One line uses one-way transitions from adaptive to non-adaptive updates, such as SWATS Keskar and Socher 2017 and bounded-adaptive schemes such as AdaBound Luo et al. 2019. Another line combines update dynamics through wrappers like Lookahead Zhang et al. 2019. A more recent line explicitly models multi-optimizer interleaving and switching; for example, IOMT (Chen et al. 2025) and DOIT (Chen et al. 2026) use surrogate performance models and acquisition-style selection rules to choose optimizers over training stages. In parallel, meta-learning approaches treat optimizer design itself as a learned problem (e.g., LSTM-based optimizers in Andrychowicz et al. 2016).

These advances are important, but they also expose a practical tradeoff: richer optimizer-selection policies can improve adaptation, yet they may increase system complexity, introduce additional tuning surfaces, and reduce plug-and-play usability in standard training pipelines. OptiRoulette is designed around a complementary point in this design space: a lightweight stochastic interleaving policy that remains optimizer-native and deployment-oriented, while still exploiting stage-dependent optimizer diversity.

Specifically, OptiRoulette is proposed as a standalone optimizer that combines (i) warmup locking, (ii) stochastic epoch-level sampling from an active optimizer pool, (iii) compatibility-aware learning-rate scaling during optimizer transitions, and (iv) failure-aware pool replacement. The optimizer is implemented as a `torch.optim.Optimizer`-compatible component intended for drop-in usage and packaging.

This paper makes four contributions. First, it formalizes the OptiRoulette optimization process as a stochastic optimizer-selection mechanism over an evolving active set. Second, it provides a theory-grounded interpretation of why the warmup-plus-interleaving regime can accelerate convergence in practice. Third, it reports completed 10-seed evidence across five image-classification suites (CIFAR-100, CIFAR-100-C, SVHN, Tiny ImageNet, and Caltech-256), with emphasis on time-to-target convergence, which is the main competitive advantage observed in this study (Section 4.1).

Fourth, it positions the resulting milestone behavior against current literature and public-archive reporting conventions.

2. OptiRoulette Optimizer Design

2.1. State and Components

Let $\mathcal{O} = \{o_1, \dots, o_K\}$ be the set of configured optimizers. At each training epoch e , OptiRoulette maintains:

1. an active set $\mathcal{A}_e \subseteq \mathcal{O}$ (from the pool manager),
2. a blocked set $\mathcal{B}_e \subseteq \mathcal{O}$,
3. a current optimizer $o_e \in \mathcal{A}_e$.

The optimizer state machine is split into phases:

1. **Warmup phase**: optimizer is locked to a predefined optimizer (SGD in our experiments),
2. **Roulette phase**: optimizer is sampled randomly from candidates.

2.2. Random Selection Rule

Candidate optimizers at epoch e are:

$$\mathcal{C}_e = \mathcal{A}_e \setminus \mathcal{B}_e, \quad (1)$$

with fallback to $\mathcal{O} \setminus \mathcal{B}_e$ if \mathcal{C}_e is empty.

With `avoid_repeat=true`, the previous optimizer is removed from candidates when possible:

$$\mathcal{C}'_e = \begin{cases} \mathcal{C}_e \setminus \{o_{e-1}\}, & \text{if } |\mathcal{C}_e| > 1, \\ \mathcal{C}_e, & \text{otherwise.} \end{cases} \quad (2)$$

The selected optimizer is sampled uniformly:

$$o_e \sim \text{Unif}(\mathcal{C}'_e). \quad (3)$$

In the reported experiments, switching granularity is `epoch`; therefore one optimizer is selected per epoch (except during warmup lock), and all batches in that epoch use the same optimizer.

2.3. Warmup and Phase Transition

Warmup can terminate in two ways:

1. fixed epoch cutoff (`warmup_epochs`),
2. plateau criterion on validation accuracy slope.

In the completed runs, fixed warmup is used with `warmup_epochs=17`, `warmup_optimizer=sgd`, and `dropafter_warmup=true`. Hence SGD is forced during early training and then excluded from roulette candidates after warmup.

2.4. Reward and Pool Replacement

After each epoch, the evaluation loop computes a reward for the selected optimizer:

$$r_e = 0.7 \cdot (\text{valAcc}_e - \text{valAcc}_{o_e}^{\text{last}}) + 0.3 \cdot (\text{valAcc}_e - \text{valAcc}^{\text{global-last}}), \quad (4)$$

then clips $r_e \in [-1, 1]$.

Pool replacement is triggered by failure conditions:

1. consecutive low rewards below a threshold,
2. catastrophic validation drop relative to best observed validation accuracy.

The replacement active optimizer is selected from backup candidates, optionally using compatibility constraints and preferred swap rules. Learning rates can be adjusted across swaps via compatibility-aware scaling rules.

2.5. Why OptiRoulette Can Converge Faster

The observed acceleration can be interpreted as a stage-wise stochastic preconditioning effect.

Let $g_t = \nabla_{\theta} \mathcal{L}(\theta_t)$ and let optimizer o_t apply update map ϕ_{o_t} with internal state $s_t^{(o_t)}$ and base learning rate η_{o_t} . The OptiRoulette update can be written as

$$\theta_{t+1} = \theta_t - \eta_{o_t} \phi_{o_t}(g_t, s_t^{(o_t)}). \quad (5)$$

Conditioned on selection probabilities $\pi_t(i) = \Pr[o_t = i]$ over active candidates, the expected update is

$$\mathbb{E}[\Delta\theta_t | g_t] = - \sum_{i \in \mathcal{A}_t} \pi_t(i) \eta_i \phi_i(g_t, s_t^{(i)}), \quad (6)$$

which behaves as a mixture of optimizer-specific descent geometries rather than a single fixed preconditioner.

In the reported configuration, this mixture is preceded by an explicit **17-epoch warmup** (`warmup_epochs=17`) with `warmup_optimizer=sgd` at LR 0.1, then SGD is removed (`dropafter_warmup=true`). This creates a two-stage dynamic:

1. **Fast basin entry:** high-step SGD warmup rapidly moves from random initialization to a useful attraction region.

2. **Refinement regime:** after warmup, selection is over {Nadam, Adam, AdamW, Ranger, Adan, Lion} with substantially smaller base LRs (Nadam/Adam/AdamW: 10^{-3} , Ranger: $7 \cdot 10^{-4}$, Adan: $1.2 \cdot 10^{-4}$, Lion: 10^{-5}), reducing oscillation while preserving optimizer diversity.

Relative to warmup LR 0.1, this induces an immediate post-warmup step-size contraction of approximately 10^2 – 10^4 , which helps convert rapid early progress into stable late-stage refinement.

Compatibility-aware LR scaling further regularizes transitions:

1. high-to-low-family transition scale: 0.01 (`from_high_to_low`),
2. low-to-high-family transition scale: 10.0 (`from_low_to_high`),
3. special cases: AdaHessian LR override 0.15, Lion LR cap $3 \cdot 10^{-4}$.

These rules are designed to limit destructive step-size discontinuities across optimizer families and to keep switched dynamics inside a stable trust region.

Finally, pool replacement and recovery settings (`failure_threshold=-0.15`, `consecutive_failure_limit=3`, `catastrophic_drop=0.3`, grace period 5 epochs, momentum transfer scaling 0.5) reduce persistence of underperforming optimizer states. The net effect is a biased random process toward stable, high-payoff update dynamics, which is consistent with the faster empirical time-to-target convergence reported in Table 4.1.

2.6. Implementation Notes

For the current settings, roulette is random over a restricted active set rather than random over all configured optimizers. A consequence of epoch-level switching is that per-epoch optimizer distribution becomes one-hot, making per-epoch strategy entropy (logged as `nash_conv/strategy_entropy`) collapse to zero.

3. Experimental Setup

3.1. Data and Architectures

Before reporting results, we summarize the concrete CNN and data-pipeline settings used in the completed runs, because convergence behavior is sensitive to both architecture and augmentation choices.

1. **CIFAR-100**: the completed run uses a ResNet-110 classifier (100 classes, initial channels 64), batch size 128, and a 0.9/0.1 train/validation split with seed 42. The augmentation stack combines random crop, random horizontal flip, cutout (size 8), and mild color jitter.

2. **CIFAR-100-C**: the completed run follows the same ResNet-110 training configuration family as CIFAR-100, while final test evaluation is performed on the corruption-shifted CIFAR-100-C distribution. This preserves a comparable training protocol and isolates distribution-shift effects at test time.

3. **SVHN**: the completed run uses ResNet-110 with initial channels 16 (10 classes), batch size 128, and a 0.9/0.1 split. Augmentation is dataset-specific (padding-4 crop, AutoAugment-SVHN policy, cutout size 16) and deliberately excludes horizontal flipping.

4. **Tiny ImageNet**: the completed run uses the SAMix architecture configuration (200 classes, initial channels 64), batch size 128, and a 0.9/0.1 train/validation split with seed 42.

5. **Caltech-256**: the completed run uses ResNet-50 (257 classes), batch size 128, an initial 0.8 train split, and then a 0.9/0.1 train/validation split. The image pipeline uses size 64, random resized crop, random horizontal flip, color jitter, and cutout.

3.2. Optimization Configuration

Common key settings across the five experiments:

1. `max_epochs=100` (CIFAR-100, CIFAR-100-C, Caltech-256) and `max_epochs=110` (SVHN, Tiny ImageNet),
2. `warmup_epochs=17, warmup_optimizer=sgd,`
3. `switch_granularity=epoch, switch_every_steps=1,`
4. `switch_probability=1.0, avoid_repeat=true,`
5. optimizer pool with 7 active optimizers: {sgd, nadam, adam, adamw, ranger, adan, lion}.

In the completed runs, optimizer-side controls are intentionally aligned across datasets: `dropafter_warmup=true, use_scheduler=false,` and gradient clipping at 2.0. Representative base learning rates in the post-warmup pool are 10^{-3} (Adam/AdamW/Nadam), $7 \cdot 10^{-4}$ (Ranger), $1.2 \cdot 10^{-4}$ (Adan), and 10^{-5} (Lion).

Taken together, this setting bundle (pool composition, learning-rate vector, warmup/switching controls, and stabilization rules) defines the default OptiRoulette experimental preset in this paper. This default was selected from internal cross-dataset tuning as the most consistently effective and stable choice on the majority of the studied datasets.

The baseline `simple` mode uses a single optimizer. In all completed runs reported here, that optimizer is AdamW (verified in per-run logs). Comparisons therefore quantify the benefit of OptiRoulette optimizer logic against a standard fixed optimizer.

3.3. Evaluation Protocol

Each experiment uses 10 distinct seeds. We report means, standard deviations, and 95% confidence intervals from the completed run suites for CIFAR-100, CIFAR-100-C, SVHN, Tiny ImageNet, and Caltech-256, using a consistent post-processing and statistical-analysis protocol across datasets.

Runs are paired by seed between modes: for each dataset, the same run index uses the same seed in `roulette` and `simple`. The mapping is identical across CIFAR-100, CIFAR-100-C, SVHN, Tiny ImageNet, and Caltech-256:

<code>run01</code>	2746317213	<code>run06</code>	127978094
<code>run02</code>	1181241943	<code>run07</code>	939042955
<code>run03</code>	958682846	<code>run08</code>	2340505846
<code>run04</code>	3163119785	<code>run09</code>	946785248
<code>run05</code>	1812140441	<code>run10</code>	2530876844

4. Results (Current Completed Runs)

4.1. Convergence Speed: Main Competitive Advantage

Using the architecture and optimization settings detailed in Section 3, the dominant practical advantage of OptiRoulette in the current experiments is convergence speed to useful validation-accuracy regimes. Table 4.1 reports headline first-hit milestones in epochs and wall-clock seconds.

Table 1 Headline Convergence Milestones (First Hit of Validation Accuracy Target)

Dataset	Mode	Target	Reach Rate	First Epoch (\downarrow)	First Time (s) (\downarrow)
CIFAR-100	Roulette	0.65	10/10	18.8	1124.1
CIFAR-100	Simple (AdamW)	0.65	10/10	25.1	1508.7
CIFAR-100	Roulette	0.75	10/10	30.4	1912.0
CIFAR-100	Simple (AdamW)	0.75	0/10	–	–
CIFAR-100-C	Roulette	0.65	10/10	18.8	1122.8
CIFAR-100-C	Simple (AdamW)	0.65	10/10	25.7	1536.9
CIFAR-100-C	Roulette	0.75	10/10	30.8	1935.8
CIFAR-100-C	Simple (AdamW)	0.75	0/10	–	–
SVHN	Roulette	0.95	10/10	18.8	887.3
SVHN	Simple (AdamW)	0.95	10/10	28.9	1369.9
SVHN	Roulette	0.96	10/10	27.1	1370.2
SVHN	Simple (AdamW)	0.96	0/10	–	–
Tiny ImageNet	Roulette	0.60	10/10	23.7	4127.1
Tiny ImageNet	Simple (AdamW)	0.60	0/10	–	–
Tiny ImageNet	Roulette	0.65	10/10	44.1	7826.4
Tiny ImageNet	Simple (AdamW)	0.65	0/10	–	–
Caltech-256	Roulette	0.59	10/10	25.7	1054.4
Caltech-256	Simple (AdamW)	0.59	10/10	77.0	3138.4
Caltech-256	Roulette	0.62	10/10	30.3	1250.6
Caltech-256	Simple (AdamW)	0.62	0/10	–	–

For shared targets, OptiRoulette reaches targets earlier on CIFAR-100/CIFAR-100-C, SVHN, and Caltech-256: CIFAR-100 at 0.65 (18.8 vs 25.1 epochs), CIFAR-100-C at 0.65 (18.8 vs 25.7), SVHN at 0.95 (18.8 vs 28.9), and Caltech-256 at 0.59 (25.7 vs 77.0, nearly $3\times$ faster). For harder targets (CIFAR-100 0.75, CIFAR-100-C 0.75, SVHN 0.96, Tiny ImageNet 0.65, Caltech-256 0.62), the baseline does not reach the same regime within budget. Using a budget-capped lower-bound framing for non-attained targets, the implied speedup reaches up to $5.3x$ (CIFAR-100/CIFAR-100-C target 0.70: 18.8 epochs vs baseline not reached by epoch 100).

To make the fast-convergence picture explicit across all completed datasets, Table 4.1 reports additional OptiRoulette milestones.

Hence, OptiRoulette reaches high validation regimes with full reach rate across all five datasets: 74%/75% on CIFAR-100 at epochs 26.3/30.4, 74%/75% on CIFAR-100-C at 25.7/30.8, 0.96 on SVHN at epoch 27.1, 0.65 on Tiny ImageNet at epoch 44.1, and 0.68 on Caltech-256 at epoch 63.7 (all 10/10 where reported). This convergence behavior, rather than only final-point accuracy, is the main competitive differentiator of OptiRoulette.

For camera-ready assembly, we reserve per-dataset figure slots for two visual diagnostics: (i) a combined train/validation accuracy-loss panel and (ii) mean ROC curves across seeds. The paths below are placeholders and can be replaced with exported notebook figures.

Table 2 Fine-Grained OptiRoulette Convergence Milestones

Dataset	Target	Reach Rate	First Epoch (\downarrow)	First Time (s) (\downarrow)
CIFAR-100	0.70	10/10	18.8	1124.1
CIFAR-100	0.72	10/10	21.1	1276.3
CIFAR-100	0.73	10/10	23.4	1432.0
CIFAR-100	0.74	10/10	26.3	1630.7
CIFAR-100	0.75	10/10	30.4	1912.0
CIFAR-100-C	0.70	10/10	18.8	1122.8
CIFAR-100-C	0.72	10/10	22.0	1335.4
CIFAR-100-C	0.73	10/10	22.5	1370.2
CIFAR-100-C	0.74	10/10	25.7	1592.4
CIFAR-100-C	0.75	10/10	30.8	1935.8
SVHN	0.93	10/10	17.7	819.7
SVHN	0.94	10/10	18.7	880.7
SVHN	0.95	10/10	18.8	887.3
SVHN	0.96	10/10	27.1	1370.2
Tiny ImageNet	0.60	10/10	23.7	4127.1
Tiny ImageNet	0.62	10/10	27.6	4831.5
Tiny ImageNet	0.63	10/10	31.8	5591.2
Tiny ImageNet	0.64	10/10	35.3	6227.7
Tiny ImageNet	0.65	10/10	44.1	7826.4
Caltech-256	0.60	10/10	27.3	1121.7
Caltech-256	0.62	10/10	30.3	1250.6
Caltech-256	0.64	10/10	36.9	1545.6
Caltech-256	0.66	10/10	43.9	1851.6
Caltech-256	0.68	10/10	63.7	2698.7

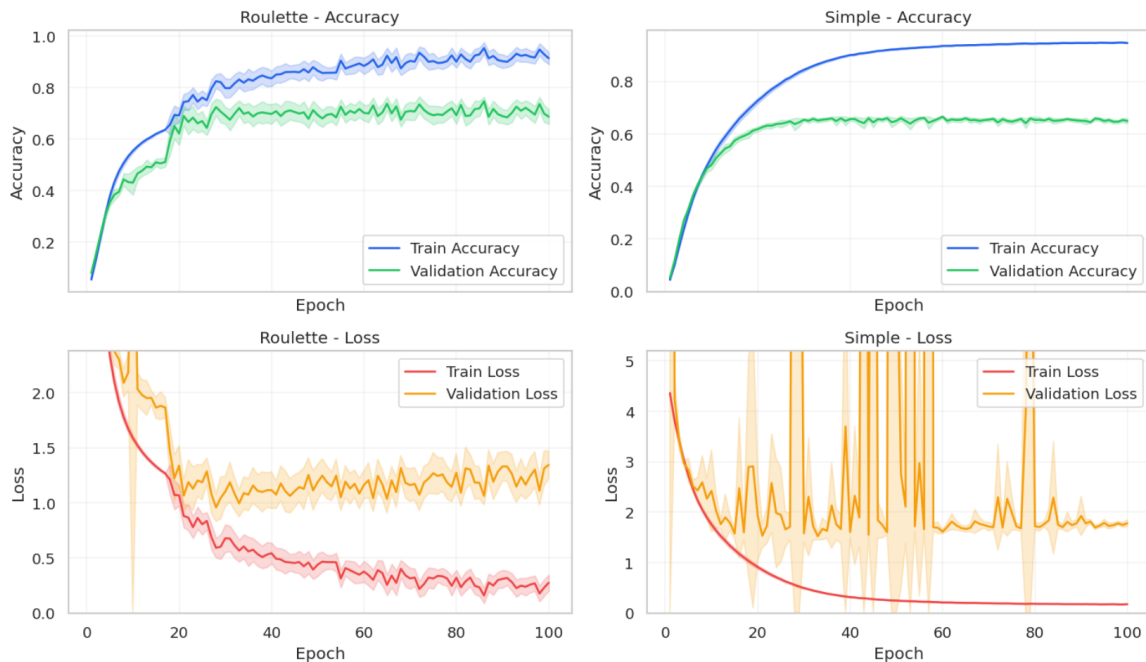


Figure 1 CIFAR-100: mean train/validation accuracy and loss trajectories across epochs for OptiRoulette and Simple (AdamW).

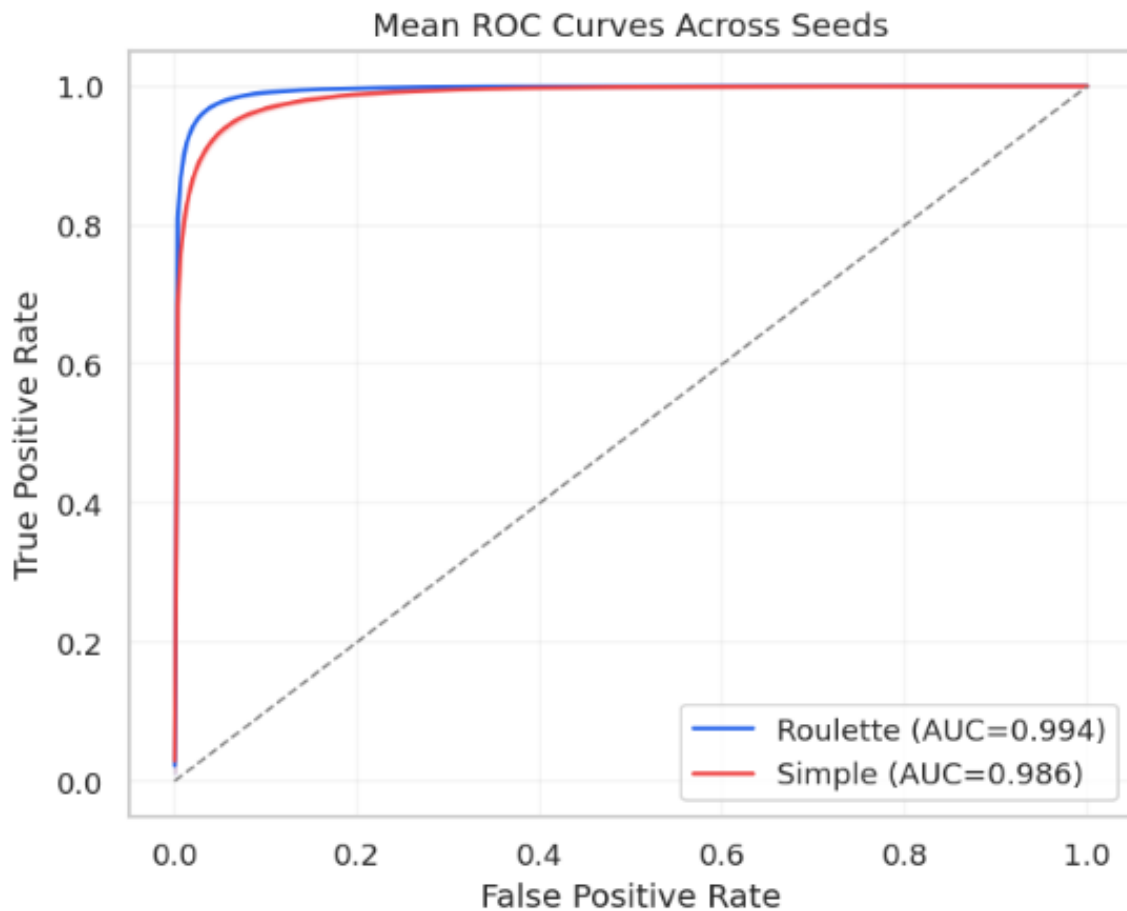


Figure 2 CIFAR-100: mean ROC curves across seeds for OptiRoulette and Simple (AdamW).

CIFAR-100 visual analysis. Figure 1 shows a clear separation in optimization dynamics after the early training phase: OptiRoulette reaches higher validation accuracy regimes earlier and then remains around a stable high plateau, whereas the fixed AdamW baseline saturates at a lower validation-accuracy level despite continued growth in training accuracy. The corresponding loss panels indicate that OptiRoulette drives validation loss to a lower and more stable operating range, while Simple (AdamW) exhibits substantially higher variance and frequent spikes in validation loss. Figure 2 is consistent with this behavior at evaluation time, with a higher mean ROC curve for OptiRoulette and a higher reported mean AUC (0.994 vs 0.986). Taken together, these plots support the interpretation that OptiRoulette’s main gain on CIFAR-100 is faster and more reliable convergence to a stronger generalization regime.

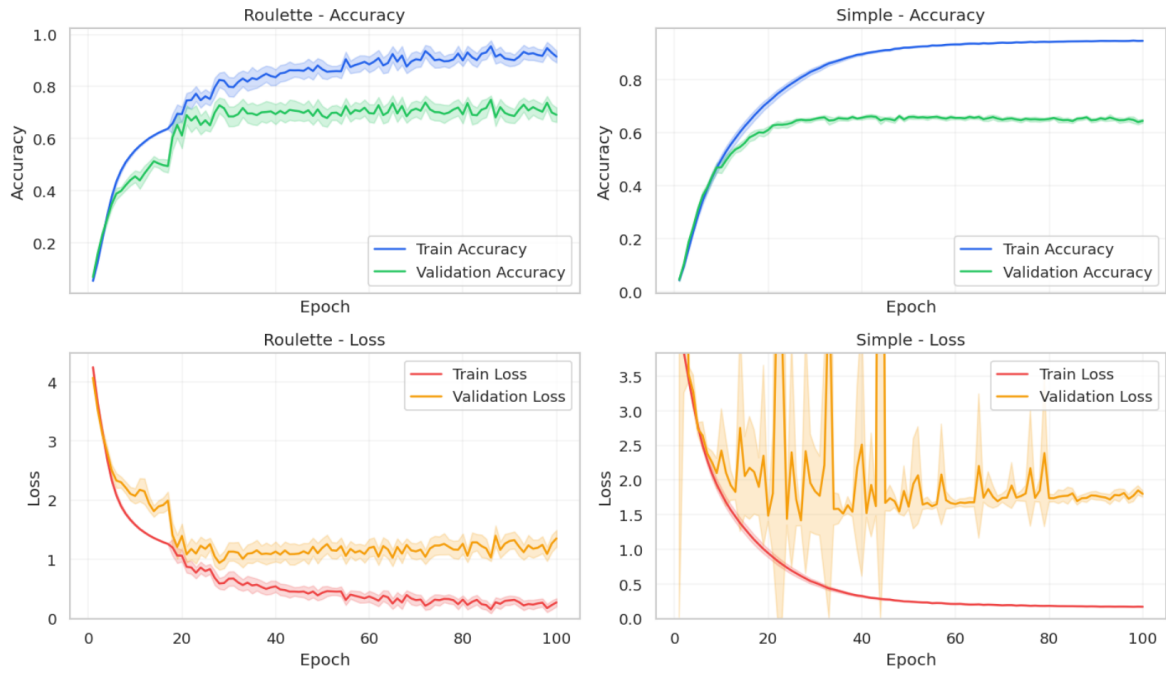


Figure 3 CIFAR-100-C: mean train/validation accuracy and loss trajectories across epochs for OptiRoulette and Simple (AdamW).

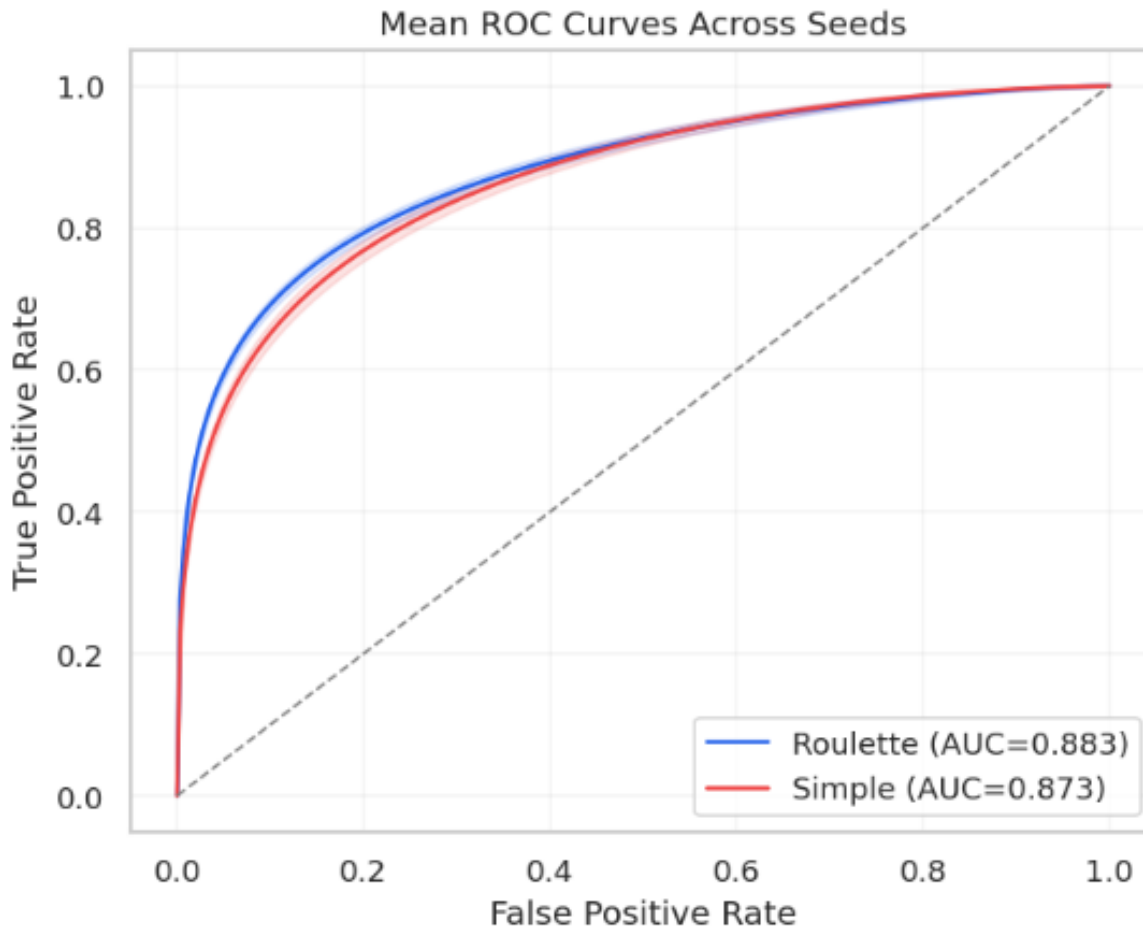


Figure 4 CIFAR-100-C: mean ROC curves across seeds for OptiRoulette and Simple (AdamW).

CIFAR-100-C visual analysis. Figure 3 reproduces the same qualitative pattern under corruption shift: OptiRoulette reaches a higher validation-accuracy band earlier and remains consistently above the fixed-optimizer baseline across the training budget. In the loss panels, OptiRoulette shows a smoother and lower validation-loss trajectory, whereas Simple (AdamW) remains noisier with larger fluctuations and recurrent spikes, indicating weaker stability under shifted test conditions. Figure 4 provides aligned ranking evidence at the classifier level, with OptiRoulette yielding a higher mean ROC curve and higher mean AUC (0.883 vs 0.873). Overall, the CIFAR-100-C plots support that the convergence and stability advantage of OptiRoulette persists beyond the in-distribution setting.

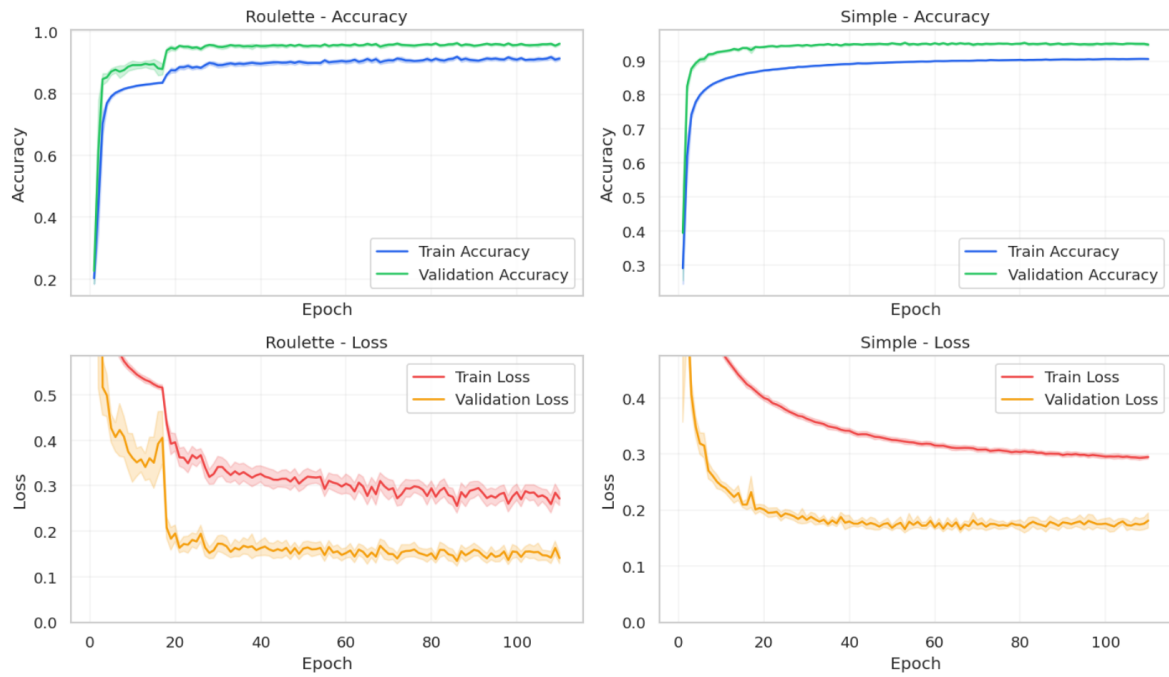


Figure 5 SVHN: mean train/validation accuracy and loss trajectories across epochs for OptiRoulette and Simple (AdamW).

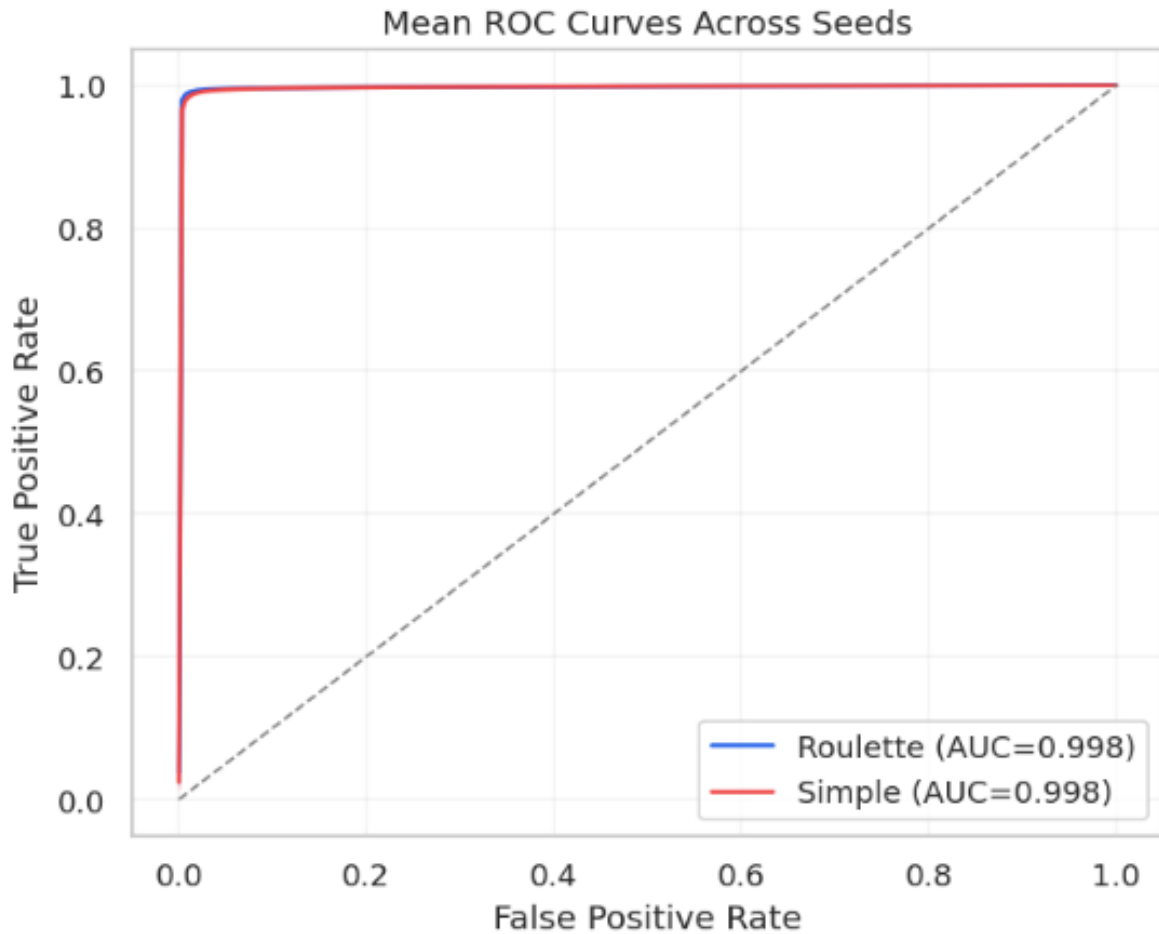


Figure 6 SVHN: mean ROC curves across seeds for OptiRoulette and Simple (AdamW).

SVHN visual analysis. Figure 5 indicates that both methods converge quickly on SVHN, but OptiRoulette still reaches high-validation regimes earlier and stabilizes at a slightly stronger operating point. A clear phase transition is visible around the warmup boundary, after which OptiRoulette’s validation loss drops and remains low with limited variance. In contrast, Simple (AdamW) improves more gradually and plateaus at a marginally weaker level. Figure 6 shows near-overlapping ROC curves and identical rounded mean AUC (0.998 vs 0.998), so the practical advantage on SVHN is primarily faster time-to-target and small but consistent accuracy gains rather than a large ROC-shape separation.

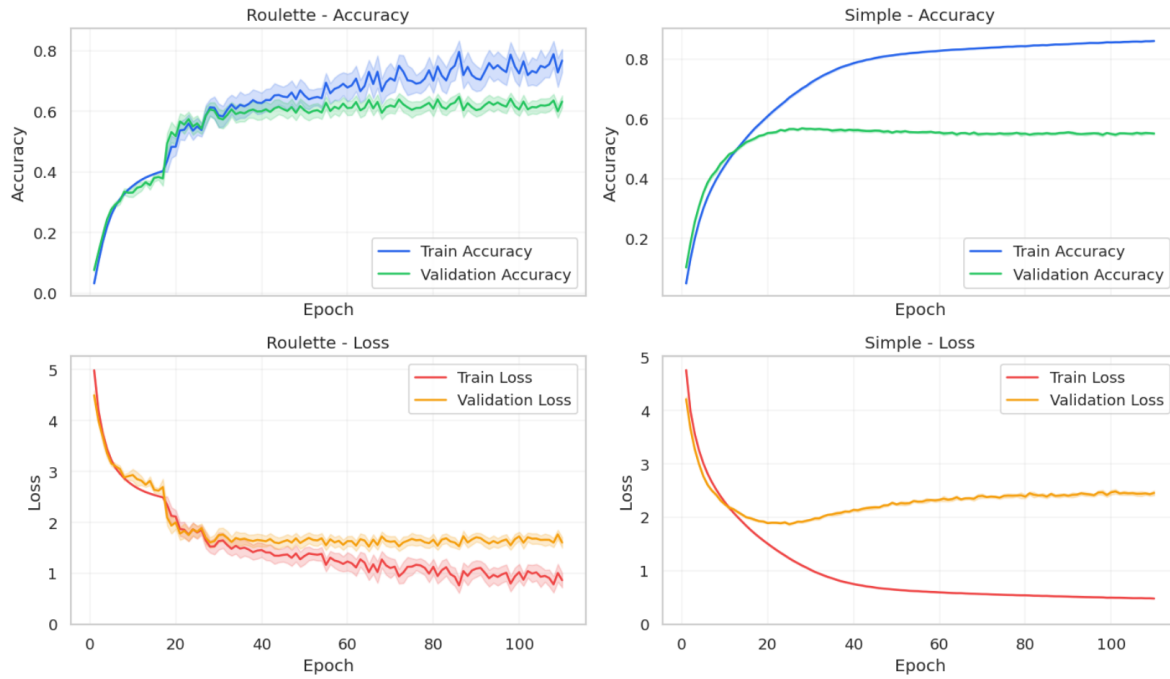


Figure 7 Tiny ImageNet: mean train/validation accuracy and loss trajectories across epochs for OptiRoulette and Simple (AdamW).

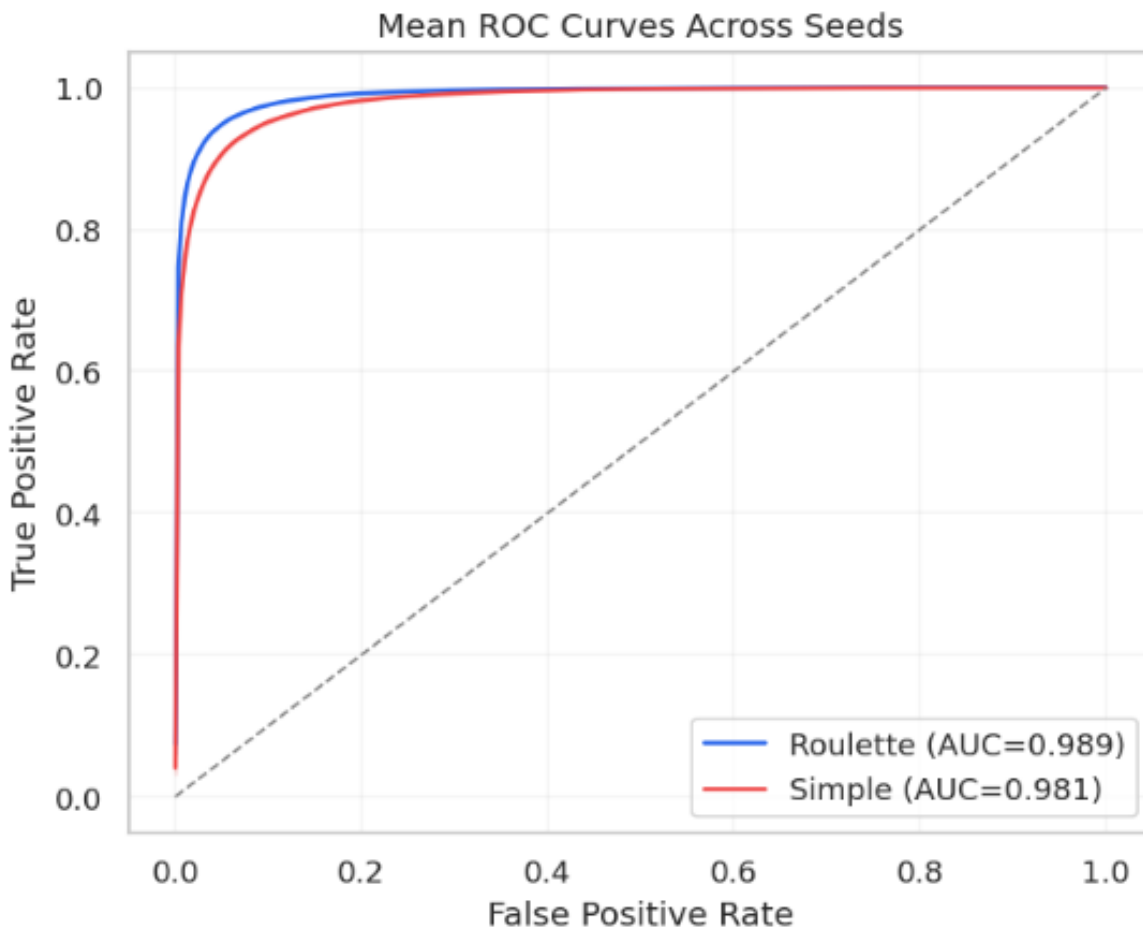


Figure 8 Tiny ImageNet: mean ROC curves across seeds for OptiRoulette and Simple (AdamW).

Tiny ImageNet visual analysis. Figure 7 highlights a strong separation in generalization dynamics on the most challenging setting of the current study. OptiRoulette continues to lift validation accuracy after the early phase and reaches a clearly higher plateau, while Simple (AdamW) saturates earlier at a substantially lower validation-accuracy level. The loss plots reinforce this interpretation: in the baseline, validation loss declines initially but then trends upward and remains high, consistent with overfitting under a fixed optimizer policy; OptiRoulette maintains a lower and more controlled validation-loss trajectory throughout training. Figure 8 is aligned with the same ranking, with a visibly better mean ROC curve and higher mean AUC for OptiRoulette (0.989 vs 0.981). These plots support the claim that OptiRoulette’s convergence advantage is especially pronounced when optimization and generalization are both difficult.

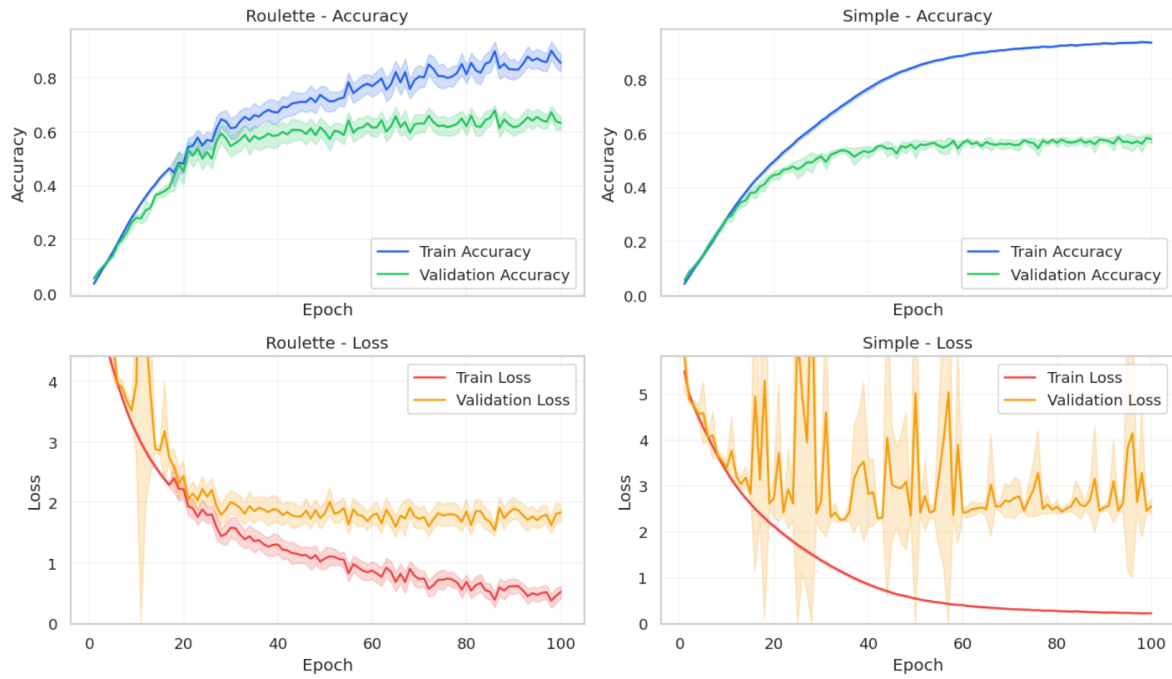


Figure 9 Caltech-256: mean train/validation accuracy and loss trajectories across epochs for OptiRoulette and Simple (AdamW).

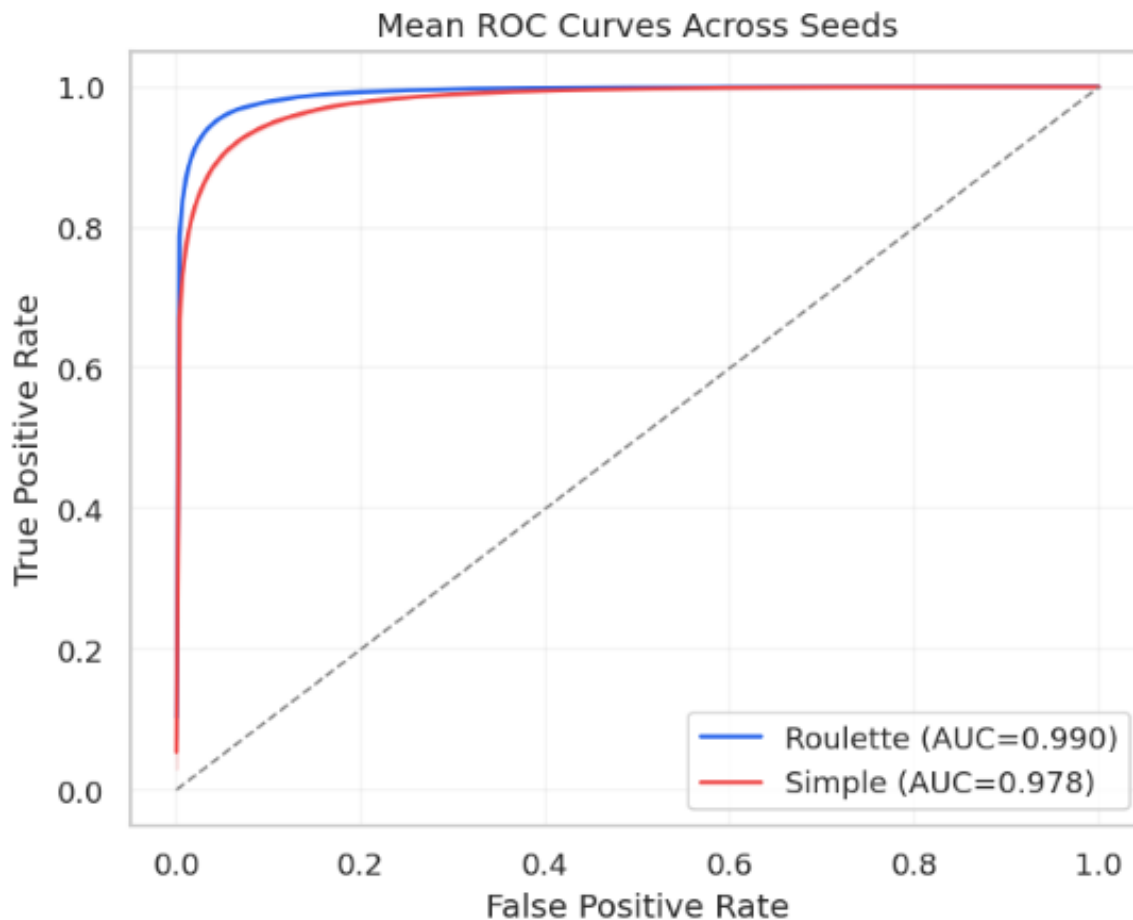


Figure 10 Caltech-256: mean ROC curves across seeds for OptiRoulette and Simple (AdamW).

Caltech-256 visual analysis. Figure 9 shows a strong convergence-gap pattern in favor of OptiRoulette: validation accuracy rises to a higher regime substantially earlier and remains clearly above the fixed AdamW baseline throughout training. The loss trajectories provide complementary evidence. Under OptiRoulette, validation loss decreases to a lower and relatively stable band, while the Simple (AdamW) run exhibits larger volatility and persistent high-amplitude spikes, indicating less robust optimization dynamics. Figure 10 confirms the same ranking from the ROC perspective, with a higher mean ROC curve and higher mean AUC for OptiRoulette (0.990 vs 0.978). Together, these plots support the claim that the optimizer-switching mechanism yields both faster attainment of useful regimes and better final discrimination quality on Caltech-256.

4.2. Aggregate Performance

Table 4.2 summarizes aggregate metrics from the five completed 10-seed studies.

OptiRoulette improves mean test accuracy by +0.0922 on CIFAR-100 (+13.69% relative), +0.0452 on CIFAR-100-C (+15.56%), +0.0089 on SVHN (+0.92%), +0.0973 on Tiny ImageNet

Table 3 Main Results Across Completed 10-Seed Runs

Dataset	Mode	Val Acc (\uparrow)	Test Acc (\uparrow)	Test ROC-AUC (\uparrow)	Duration (s)
CIFAR-100	Roulette	0.7705 ± 0.0018	0.7656 ± 0.0024	0.99396 ± 0.00020	6678.7 ± 73.6
CIFAR-100	Simple (AdamW)	0.6792 ± 0.0033	0.6734 ± 0.0038	0.98640 ± 0.00085	5993.1 ± 29.0
CIFAR-100-C	Roulette	0.7722 ± 0.0031	0.3355 ± 0.0046	0.88291 ± 0.00628	6658.0 ± 61.1
CIFAR-100-C	Simple (AdamW)	0.6781 ± 0.0033	0.2904 ± 0.0068	0.87341 ± 0.00779	5963.5 ± 25.6
SVHN	Roulette	0.9666 ± 0.0005	0.9756 ± 0.0004	0.99792 ± 0.00005	6234.6 ± 104.7
SVHN	Simple (AdamW)	0.9578 ± 0.0006	0.9667 ± 0.0013	0.99769 ± 0.00007	5206.5 ± 26.5
Tiny ImageNet	Roulette	0.6675 ± 0.0020	0.6642 ± 0.0020	0.98854 ± 0.00013	19729.8 ± 80.4
Tiny ImageNet	Simple (AdamW)	0.5735 ± 0.0010	0.5669 ± 0.0030	0.98062 ± 0.00053	18993.1 ± 26.0
Caltech-256	Roulette	0.7001 ± 0.0020	0.6920 ± 0.0045	0.98962 ± 0.00026	4251.7 ± 127.1
Caltech-256	Simple (AdamW)	0.6014 ± 0.0057	0.5946 ± 0.0053	0.97786 ± 0.00075	4071.0 ± 85.2

Val/Test metrics are mean \pm 95% CI. Duration is mean \pm std from run-level cumulative training-time logs.

Table 4 Additional Test Metrics Across Completed 10-Seed Runs

Dataset	Mode	Test Precision (\uparrow)	Test Recall (\uparrow)	Test F1 (\uparrow)
CIFAR-100	Roulette	0.7685 ± 0.0026	0.7656 ± 0.0024	0.7657 ± 0.0024
CIFAR-100	Simple (AdamW)	0.6985 ± 0.0027	0.6734 ± 0.0038	0.6732 ± 0.0040
CIFAR-100-C	Roulette	0.4509 ± 0.0037	0.3355 ± 0.0046	0.3572 ± 0.0046
CIFAR-100-C	Simple (AdamW)	0.4103 ± 0.0053	0.2904 ± 0.0068	0.3035 ± 0.0067
SVHN	Roulette	0.9757 ± 0.0004	0.9756 ± 0.0004	0.9756 ± 0.0004
SVHN	Simple (AdamW)	0.9648 ± 0.0013	0.9644 ± 0.0016	0.9645 ± 0.0013
Tiny ImageNet	Roulette	0.6684 ± 0.0019	0.6642 ± 0.0020	0.6636 ± 0.0020
Tiny ImageNet	Simple (AdamW)	0.5990 ± 0.0021	0.5669 ± 0.0030	0.5664 ± 0.0027
Caltech-256	Roulette	0.7058 ± 0.0040	0.6920 ± 0.0045	0.6909 ± 0.0045
Caltech-256	Simple (AdamW)	0.6128 ± 0.0063	0.5584 ± 0.0049	0.5583 ± 0.0065

Entries are mean \pm 95% CI.

(+17.16%), and +0.0974 on Caltech-256 (+16.38%). Runtime overhead is +11.01% (CIFAR-100), +11.64% (CIFAR-100-C), +19.75% (SVHN), +3.88% (Tiny ImageNet), and +4.44% (Caltech-256).

4.3. Additional Test Metrics: Precision, Recall, and F1

Table 4.3 adds test precision/recall/F1 across all completed datasets. Because the current implementation uses weighted averaging for roulette and macro averaging for simple mode, these metrics should be interpreted as complementary descriptive evidence (see Threats to Validity), while accuracy and ROC-AUC remain the primary like-for-like comparison metrics.

4.4. Paired-Seed Effect Size

Because each seed is evaluated in both modes, paired differences provide a stronger comparison. Table 4.4 reports roulette minus simple deltas.

All confidence intervals remain strictly positive, indicating robust gains across seeds. For formal hypothesis testing, Table 4.4 reports paired two-sided t-tests on the same matched seeds.

Most tested metric deltas are statistically significant ($p < 0.001$). The one exception is CIFAR-100-C test ROC-AUC ($p = 0.08697$), where the current 10-seed evidence is inconclusive.

Table 5 Paired t-Tests for Test Precision, Recall, and F1 (Roulette – Simple)

Dataset	Metric	Δ Mean \pm 95% CI	$t(9)$	p -value
CIFAR-100	Test Precision	0.06998 ± 0.00305	45.00	6.61×10^{-12}
CIFAR-100	Test Recall	0.09215 ± 0.00348	51.85	1.85×10^{-12}
CIFAR-100	Test F1	0.09253 ± 0.00367	49.40	2.86×10^{-12}
CIFAR-100-C	Test Precision	0.04067 ± 0.00696	11.45	1.15×10^{-6}
CIFAR-100-C	Test Recall	0.04518 ± 0.00884	10.02	3.52×10^{-6}
CIFAR-100-C	Test F1	0.05367 ± 0.00920	11.44	1.16×10^{-6}
SVHN	Test Precision	0.01084 ± 0.00127	16.70	4.43×10^{-8}
SVHN	Test Recall	0.01127 ± 0.00175	12.64	4.95×10^{-7}
SVHN	Test F1	0.01117 ± 0.00136	16.07	6.18×10^{-8}
Tiny ImageNet	Test Precision	0.06943 ± 0.00210	64.83	2.50×10^{-13}
Tiny ImageNet	Test Recall	0.09726 ± 0.00249	76.62	5.56×10^{-14}
Tiny ImageNet	Test F1	0.09719 ± 0.00231	82.48	2.87×10^{-14}
Caltech-256	Test Precision	0.09301 ± 0.00618	29.51	2.88×10^{-10}
Caltech-256	Test Recall	0.13360 ± 0.00659	39.75	2.01×10^{-11}
Caltech-256	Test F1	0.13259 ± 0.00672	38.66	2.57×10^{-11}

Table 6 Paired Seed Deltas (Roulette – Simple)

Dataset	Δ Val Acc	Δ Test Acc	Δ Test ROC-AUC
CIFAR-100	0.0913 ± 0.0033	0.0922 ± 0.0035	0.0076 ± 0.0008
CIFAR-100-C	0.0941 ± 0.0055	0.0452 ± 0.0088	0.0095 ± 0.0097
SVHN	0.0088 ± 0.0010	0.0089 ± 0.0014	0.00023 ± 0.00005
Tiny ImageNet	0.0940 ± 0.0024	0.0973 ± 0.0025	0.0079 ± 0.0006
Caltech-256	0.0987 ± 0.0058	0.0974 ± 0.0066	0.0118 ± 0.0009

Entries are mean paired delta \pm 95% CI over 10 matched seeds.

Table 7 Paired t-Test Results (Roulette – Simple, 10 Matched Seeds)

Dataset	Metric	Δ Mean \pm 95% CI	$t(9)$	p -value
CIFAR-100	Val Acc	0.0913 ± 0.0033	54.58	1.17×10^{-12}
CIFAR-100	Test Acc	0.0922 ± 0.0035	51.85	1.85×10^{-12}
CIFAR-100	Test ROC-AUC	0.00756 ± 0.00082	18.10	2.19×10^{-8}
CIFAR-100-C	Val Acc	0.0941 ± 0.0055	33.31	9.77×10^{-11}
CIFAR-100-C	Test Acc	0.04518 ± 0.00884	10.02	3.52×10^{-6}
CIFAR-100-C	Test ROC-AUC	0.00950 ± 0.00970	1.92	8.70×10^{-2}
SVHN	Val Acc	0.00880 ± 0.00096	17.99	2.30×10^{-8}
SVHN	Test Acc	0.00893 ± 0.00138	12.73	4.66×10^{-7}
SVHN	Test ROC-AUC	0.000233 ± 0.000052	8.83	9.96×10^{-6}
Tiny ImageNet	Val Acc	0.0940 ± 0.0024	75.85	6.09×10^{-14}
Tiny ImageNet	Test Acc	0.0973 ± 0.0025	76.62	5.56×10^{-14}
Tiny ImageNet	Test ROC-AUC	0.00792 ± 0.00057	27.13	6.08×10^{-10}
Caltech-256	Val Acc	0.09869 ± 0.00581	33.30	9.79×10^{-11}
Caltech-256	Test Acc	0.09740 ± 0.00662	28.82	3.55×10^{-10}
Caltech-256	Test ROC-AUC	0.01176 ± 0.00088	26.23	8.20×10^{-10}

4.5. Validation Milestones

Milestone analysis from per-epoch logs is consistent with the convergence-centric interpretation in Tables 4.1 and 4.1: OptiRoulette repeatedly reaches higher validation-accuracy regimes that are unreachable for the single AdamW baseline within the same training budget.

4.6. Literature and Public-Archive Context

To position these convergence milestones objectively, we extended the targeted scan (as of February 20, 2026) across representative literature and public result archives for all five datasets.

Across these sources, two stable reporting patterns appear consistently: first, published and archived results are predominantly reported as endpoint metrics (final top-1 accuracy or test error), rather than as epoch-threshold first-hit milestones; second, many public training recipes use substantially longer schedules (e.g., 200/400/1800 epochs in hysts 2026) than the budgets used in the present study.

At the dataset level, the same endpoint-centric tendency remains visible. For CIFAR-100, canonical papers and benchmark archives (He et al. 2016, Zagoruyko and Komodakis 2016, Huang et al. 2017, OpenCodePapers 2026a) largely report final outcomes without first-hit milestone timing. For CIFAR-100-C, we did not find directly comparable first-hit convergence reporting; the dominant framing emphasizes post-training corruption robustness (Hendrycks and Dietterich 2019). For SVHN, both foundational papers and public leaderboard-style archives (Netzer et al. 2011, Sermanet et al. 2012, Goodfellow et al. 2013, Papers with Code 2026a) similarly focus on final accuracy. Tiny ImageNet reporting (Kim et al. 2021, OpenCodePapers 2026b) also centers on final model quality under fixed budgets. For Caltech-256, the literature and archives are often protocol-driven (train-images-per-class splits with repeated random sampling and mean recognition rates) rather than first-hit milestone-driven (Griffin et al. 2007, Bosch and Zisserman 2008), while modern deep-learning studies are frequently transfer/fine-tuning oriented (Donahue et al. 2014, Ge and Yu 2017).

Within this expanded scan, we did not find directly documented public reports with matched first-hit milestone framing for targets such as CIFAR-100/CIFAR-100-C 74%–75% by epoch ≤ 31 , SVHN 0.96 by epoch ≤ 30 , Tiny ImageNet 0.65 by epoch ≤ 45 , or Caltech-256 0.62 by epoch ≤ 35 under comparable from-scratch constraints. This is an evidence-based “not found in scanned sources” statement, not a universal impossibility claim.

5. Discussion

The current results suggest that OptiRoulette, viewed as a stochastic meta-optimizer, can provide large and stable gains over a fixed AdamW baseline, even when the internal sampling policy is simple (uniform random choice over a constrained active set). A plausible explanation is that

optimizer diversity regularizes training dynamics and reduces persistent failure modes associated with a single update rule.

A practical tradeoff is runtime overhead, especially in SVHN and the CIFAR-family runs. Nevertheless, the observed accuracy gains and milestone reliability improvements are large compared to the additional wall-clock cost.

6. Threats to Validity and Current Limitations

This section summarizes current implementation limitations and scope boundaries:

1. **Baseline scope:** current baseline is single AdamW only; stronger multi-baseline comparisons (e.g., SGD, Nadam, Ranger, Adan) remain to be completed. Additional comparisons against learning-rate schedule setups are also a relevant next step.

2. **Dataset scope:** this study reports five completed benchmark suites that were selected as comparatively larger/more challenging image-classification settings. Evaluation on simpler benchmarks (e.g., MNIST, Fashion-MNIST) has not yet been completed and remains future work.

3. **Model-family scope:** OptiRoulette has not yet been evaluated on large language model (LLM) pretraining or instruction-tuning workloads. Extending the same convergence-oriented analysis to transformer/LLM settings is planned future work.

7. Conclusion

OptiRoulette demonstrates that a warmup-plus-random-selection optimizer can outperform a fixed optimizer baseline on five multi-seed image classification benchmarks (CIFAR-100, CIFAR-100-C, SVHN, Tiny ImageNet, Caltech-256). Beyond final accuracy, the most interesting empirical signal is convergence reliability at high targets: milestones such as CIFAR-100/CIFAR-100-C 74%/75%, SVHN 0.96, Tiny ImageNet 0.65, and Caltech-256 0.62 are reached with strong consistency, while the fixed AdamW baseline does not reach several of these targets within budget. For shared targets, substantial acceleration is also observed (e.g., Caltech-256 at 0.59), and under budget-capped framing the target-attainment speedup lower bound reaches up to 5.3x (CIFAR-100/CIFAR-100-C 0.70). These first-hit milestone patterns were not directly found in our targeted public/literature scan under comparable settings (Section 4.6), making OptiRoulette a compelling candidate for time-constrained training regimes. The optimizer is already implemented as a drop-in class and can be packaged as a standalone pip-installable optimizer module (e.g., `pip install optiroulette`). The next step is to expand baseline coverage and finalize broader benchmark tables before submission.

Acknowledgments

This paper is based on internal OptiRoulette optimizer implementations and completed multi-run experimental logs.

References

- He K, Zhang X, Ren S, Sun J (2016) Deep residual learning for image recognition. In: Proceedings of CVPR. arXiv preprint: <https://arxiv.org/abs/1512.03385>.
- Zagoruyko S, Komodakis N (2016) Wide residual networks. In: Proceedings of BMVC. arXiv preprint: <https://arxiv.org/abs/1605.07146>.
- Huang G, Liu Z, Van Der Maaten L, Weinberger KQ (2017) Densely connected convolutional networks. In: Proceedings of CVPR. arXiv preprint: <https://arxiv.org/abs/1608.06993>.
- Kim M, Han D, Chun S, Han B (2021) UPANets: Learning from the universal pixel attention. arXiv preprint: <https://arxiv.org/abs/2102.02407>.
- OpenCodePapers (2026a) CIFAR-100 benchmark page (public archive of final benchmark scores). <https://opencodepapers.com/benchmarks/cifar-100>. Accessed February 17, 2026.
- OpenCodePapers (2026b) Tiny ImageNet benchmark page (public archive of final benchmark scores). <https://opencodepapers.com/benchmarks/tiny-imagenet>. Accessed February 17, 2026.
- hysts (2026) `pytorch_image_classification` repository. Benchmark tables report test errors at last epochs and include long schedules (e.g., 200/400/1800 epochs). https://github.com/hysts/pytorch_image_classification. Accessed February 17, 2026.
- Netzer Y, Wang T, Coates A, Bissacco A, Wu B, Ng AY (2011) Reading digits in natural images with unsupervised feature learning. NIPS Workshop on Deep Learning and Unsupervised Feature Learning. http://ufldl.stanford.edu/housenumbers/nips2011_housenumbers.pdf.
- Sermanet P, Chintala S, LeCun Y (2012) Convolutional neural networks applied to house numbers digit classification. arXiv preprint <https://arxiv.org/abs/1204.3968>.
- Goodfellow IJ, Warde-Farley D, Mirza M, Courville A, Bengio Y (2013) Maxout networks. In: Proceedings of ICML. arXiv preprint <https://arxiv.org/abs/1302.4389>.
- Papers with Code (2026a) SVHN benchmark page (image classification leaderboard style archive). <https://paperswithcode.com/sota/image-classification-on-svhn>. Accessed February 20, 2026.
- Griffin G, Holub A, Perona P (2007) Caltech-256 object category dataset. California Institute of Technology Technical Report CNS-TR-2007-001. <https://authors.library.caltech.edu/records/5sv1j-ytw97>.
- Bosch A, Zisserman A (2008) Caltech-256 results page (public benchmark archive and protocol details). https://www.robots.ox.ac.uk/~7Evgg/research/caltech/C256_graph.html. Accessed February 20, 2026.
- Donahue J, Jia Y, Vinyals O, Hoffman J, Zhang N, Tzeng E, Darrell T (2014) DeCAF: A deep convolutional activation feature for generic visual recognition. In: Proceedings of ICML (PMLR 32(1):647–655). <https://proceedings.mlr.press/v32/donahue14.html>.

-
- Ge W, Yu Y (2017) Borrowing treasures from the wealthy: Deep transfer learning through selective joint fine-tuning. In: Proceedings of CVPR. arXiv preprint <https://arxiv.org/abs/1702.08690>.
- Hendrycks D, Dietterich T (2019) Benchmarking neural network robustness to common corruptions and perturbations. In: Proceedings of ICLR. arXiv preprint <https://arxiv.org/abs/1903.12261>.
- Chen Y, Wen Z, Chen J, Huang J (2025) Interleaving optimizers for DNN training. ICLR 2025 submission. <https://openreview.net/forum?id=uApm5otXfH>.
- Chen Y, Wen Z, Chen J, Huang J (2026) Towards dynamic interleaving optimizers. ICLR 2026 poster. <https://openreview.net/forum?id=AI18ADdDht>.
- Keskar NS, Socher R (2017) Improving generalization performance by switching from Adam to SGD. arXiv preprint <https://arxiv.org/abs/1712.07628>.
- Luo L, Xiong Y, Liu Y, Sun X (2019) Adaptive gradient methods with dynamic bound of learning rate. In: Proceedings of ICLR. <https://openreview.net/forum?id=Bkg3g2R9FX>.
- Zhang MR, Lucas J, Hinton G, Ba J (2019) Lookahead optimizer: k steps forward, 1 step back. In: Proceedings of NeurIPS. <https://arxiv.org/abs/1907.08610>.
- Andrychowicz M, Denil M, Gomez S, Hoffman MW, Pfau D, Schaul T, Shillingford B, de Freitas N (2016) Learning to learn by gradient descent by gradient descent. In: Proceedings of NeurIPS. <https://arxiv.org/abs/1606.04474>.
- Krizhevsky A (2009) Learning multiple layers of features from tiny images. Technical report, University of Toronto.
- Le Y, Yang X (2015) Tiny ImageNet visual recognition challenge. Stanford CS231N project report.
- Kingma DP, Ba J (2015) Adam: A method for stochastic optimization. In: Proceedings of ICLR.
- Loshchilov I, Hutter F (2019) Decoupled weight decay regularization. In: Proceedings of ICLR.